Phase Diagram Studies on the Al–Ni System

K. Hilpert *, D. Kobertz *, V. Venugopal [+], M. Miller [++], H. Gerads *,
F. J. Bremer **, and H. Nickel *

* Institute for Reactor Materials, Nuclear Research Centre (KFA) Jülich, Federal Republic of Germany
** Institute for Solid State Physics, Nuclear Research Centre (KFA) Jülich

Z. Naturforsch. **42a**, 1327–1332 (1987); received August 13, 1987

Dedicated to Professor Dr. K. G. Weil on the Occasion of his 60th Birthday

The Al–Ni phase diagram has been investigated in the composition range $x_{Ni} = 0.70$ to 0.97. Phase boundaries were determined by using differential thermal analysis and Knudsen effusion mass spectrometry. The measurements were carried out in the temperature range between 1409 and 1730 K. An Al–Ni phase diagram is obtained for $x_{Ni} \geqq 0.70$ by combining the data from this work with selected data from the literature. This diagram deviates from that recommended by phase diagram compilations and used generally in the literature to date; it agrees reasonably well with a diagram which has been rejected in the literature.

1. Introduction

The nickel-rich part of the Al–Ni phase diagram is of fundamental interest for nickel-base superalloys since the yield strength of the intermetallic compound $AlNi_3$ (γ' phase) increases anomalously if the temperature rises [1]. This part of the phase diagram is also of key interest for recent research into the development of ordered alloys as new structural high-temperature materials [2]. The nickel-aluminides are considered to be important model materials for this research.

In spite of the stated importance of the nickel rich part of the Al–Ni phase diagram, a decision about very contradictory results especially for concentrations of and near the compound $AlNi_3$ [3, 4] has not yet been reached. Figure 1 shows a section of the phase diagram in the compilation of Hansen and Anderko [4]. Subsequent critical compilations (e.g. [5–8]) confirmed this phase diagram section. It is generally used in the literature to date. Recently, however, Bremer et al. [9] prepared nickel-rich $AlNi_3$ single crystals and made phase studies. Their results support the phase diagram proposed by Schramm [10], which has essentially been rejected by Hansen and Anderko [4]. According to Schramm the following peritectic and eutectic reactions exist:

$$L + \gamma[(Ni)] \rightleftharpoons \gamma'[AlNi_3] \text{ at } 1635\,K,$$

$$L \rightleftharpoons \gamma'[AlNi_3] + \beta[AlNi] \text{ at } 1633\,K.$$

These reactions differ substantially from those given by Figure 1:

$$L + \beta[AlNi] \rightleftharpoons \gamma'[AlNi_3] \text{ at } 1668\,K,$$

$$L \rightleftharpoons \gamma[(Ni)] + \gamma'[AlNi_3] \text{ at } 1658\,K.$$

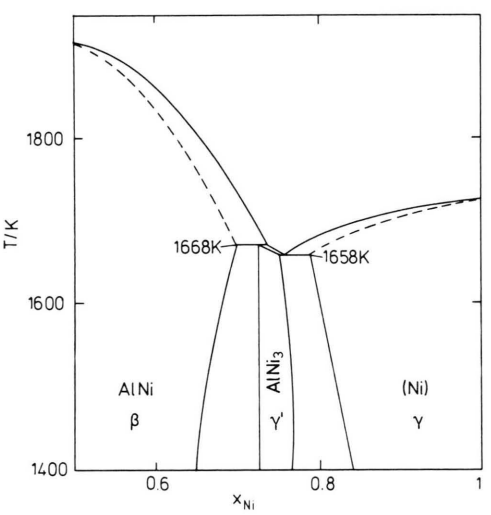

Fig. 1. Ni rich part of the Al–Ni phase diagram according to Hansen and Anderko [4].

[+] On leave from: Fuel Chemistry Division, Bhabha Atomic Research Centre, Bombay 400085, India.
[++] On leave from: Technical University of Wrocław, Wybrzeże S. Wyspiańskiego 27, 50-370 Wrocław, Poland.

Reprint requests to PD Dr. K. Hilpert, Institute for Reactor Materials, Nuclear Research Centre (KFA) Jülich, P.O. Box 1913, D-5170 Jülich, Federal Republic of Germany.

0932-0784 / 87 / 1100-1327 $ 01.30/0. – Please order a reprint rather than making your own copy.

To clarify the contradictory results, phase boundaries were determined for alloys of the compositions $\{x\,\mathrm{Ni} + (1-x)\,\mathrm{Al}\}$, $x = 0.700$ to 0.970. High precision differential thermal analysis and Knudsen effusion mass spectrometry were used for the first time in these investigations. Thermodynamic properties determined additionally for the melts and the solid phases of this composition range will be given in a separate publication [11].

2. Experimental

2.1 Samples

Alloy samples of different composition were prepared by induction melting in a purified argon atmosphere using the levitation technique. Nickel (purity 99.98 mass per cent, supplied by Société Metallurgique le Nickel-SLN, Paris, France, after vacuum degassing 99.997 mass per cent) and aluminium (purity 99.999 mass per cent, supplied by VAW Aluminium, Bonn, Federal Republic of Germany) were used as starting materials. Quantitative analysis of the samples by atomic absorption spectroscopy yielded the original weighed-in quantities of the components within the uncertainty of the analysis amounting to about $\pm$ 0.5%.

Twenty-one samples with $x_{\mathrm{Ni}} = 0.700$, 0.710, 0.720, ..., 0.850, 0.880, 0.910, 0.940, 0.970, and 0.755 were thus obtained.

2.2 Differential Thermal Analysis

The thermal analyzer used for the measurements (model 429, Netzsch, Selb, Federal Republic of Germany) renders possible simultaneous differential thermal analysis and thermogravimetric analysis. The alloy samples were heated in alumina crucibles with a high-temperature furnace, model 62253-03, Netzsch, under flowing helium (purity 99.9999 vol.%) at a flow rate of $80\,\mathrm{nm^3\,s^{-1}}$. Traces of moisture and oxygen were removed by passing the gas through a molecular sieve and calcium at 550 K before it entered the analyzer. In addition, zirconium foil was arranged near the sample as an "in situ" getter for oxygen and moisture. All gas connections were made using 6 mm diameter teflon tubes with high vacuum connectors. The temperature measurement with Pt/Pt + 10% Rh thermocouples was calibrated by the melting points of silver, gold, and nickel as given by the International Practical Temperature Scale [12]. 650 mg of high purity platinum foil served as a reference during the measurements carried out with alloy samples with a mass of 200 to 300 mg.

2.3 Knudsen Effusion Mass Spectrometry

The measurements were carried out with a substantially modified [13, 14] Knudsen cell-mass spectrometer system supplied by Finnigan MAT, Bremen, Federal Republic of Germany. The mass spectrometer is a single focusing 90° sector field instrument of the type CH 5. The vapour species were ionized with an electron emission current of 82 μA and an electron energy of 17 to 19 eV.

Figure 2 shows the selected cylindrical Knudsen cell used in the measurements. The outer molybdenum cell contains an inner cell with a crucible, both made of high density zirconia stabilized by calcium oxide, type ZR 23, supplied by Friedrichsfeld, Mannheim, Federal Republic of Germany. Inner cells and crucibles of alumina or glassy carbon used tentatively were rejected. Alumina generates Al^+ ion intensities at the temperature of the measurements thereby reducing the sensitivity of the instrument for the detection of Al partial pressures. A solution of carbon in solid Al/Ni alloys was observed during their vaporization in cells made of glassy carbon thereby falsifying the results.

Temperatures were measured with an automatic optical pyrometer, type: mark II, Leeds & Northrup, on the bottom of a black body cavity laterally placed close to and below the bottom of the cell (see Figure 2). The temperature measurement was calibrated using the melting points of silver, gold, nickel, and platinum.

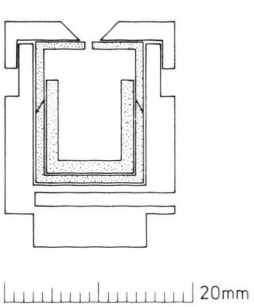

Fig. 2. Knudsen cell composed of an outer metallic cell and an inner ceramic cell with ceramic crucible.

3. Results

3.1 Differential Thermal Analysis

Investigations by differential thermal analysis were carried out at temperatures above 1600 K for all samples given in Section 2.1. Figure 3 shows a typical DTA diagram. With the exception of the sample with $x_{Ni} = 0.760$ (Fig. 4), solidus temperatures were obtained by heating the alloy samples at a rate of 2 and/or 5 K min^{-1}. The temperature indicating the beginning of melting was evaluated by the determination of the intersection of the extrapolated base line and the tangent at the point with the greatest slope on the leading edge of the endothermic peak. Liquidus temperatures were obtained in an analogous way from the exothermic peaks (cf. Fig. 3) after ascertaining that there was no detectable supercooling of the melt. This was carried out by cooling the same sample at different rates between 2 and 0.2 K min^{-1}. Only solidus temperatures are determined for the compositions $x_{Ni} \geqq 0.85$.

Eutectic temperatures in K were obtained as 1642 (0.710), 1643 (0.720), 1642 (0.730), 1642 (0.740), 1642 (0.750), and 1642 (0.755) for the compositions x_{Ni} given in parenthesis (cf. Figure 7). Peritectic temperatures resulted for samples with $x_{Ni} = 0.755$, 0.760, 0.770, and 0.780 as 1645, 1646, 1645, and 1644 K, respectively.

All temperatures determined here by differential thermal analysis for alloy samples of different compositions are shown in Figure 7.

The two methods used for temperature determination, by heating and by cooling, yielded two values for the melting point of gold which agree excellently within the precision of these determinations ($\pm$ 0.5 K). This shows the potential of the evaluation method employed.

Thermogravimetric analyses were carried out with a sensitivity of 50 µg at the same time as the investigations by differential thermal analysis. No weight change was observed during the measurements.

3.2 Knudsen Effusion Mass Spectrometry

Upon vaporizing the alloy samples of the compositions given in Sect. 2.1 with the exception of those with $x_{Ni} = 0.710$, 0.720, 0.755, 0.780, 0.810, 0.820, and 0.840 the ions Ni^+ and Al^+ were detected. These ions are formed in the ion source from the gaseous species

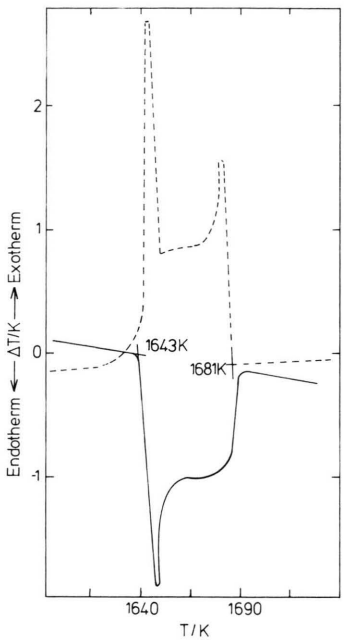

Fig. 3. DTA for an alloy with $x_{Ni} = 0.720$ (— heating with a rate of 5 K min^{-1}; - - - cooling with a rate of 5 K min^{-1}; sample weight 250 mg).

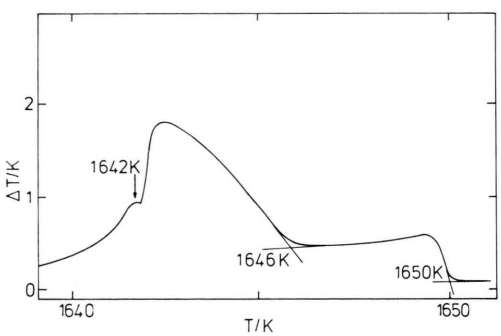

Fig. 4. DTA for an alloy with $x_{Ni} = 0.760$ obtained by cooling with a rate of 0.5 K min^{-1}.

Ni(g) and Al(g) according to the reactions

$$Ni(g) + e^- \rightarrow Ni^+ + 2e^-,$$
$$Al(g) + e^- \rightarrow Al^+ + 2e^-.$$

The Ni^+ and Al^+ ion intensities are proportional to the Ni and Al equilibrium partial pressures over the alloys [15]. The presence of thermodynamic equilibrium in the Knudsen cell was shown by measurements with different sample surface area/effusion orifice area ratios.

Ni^+/Al^+ ion intensity ratios were determined over solid alloy samples of different compositions in the temperature range between 1409 and 1703 K. The essential results for the evaluation in this work are shown in Figure 5. According to the phase rule the Ni and Al partial pressures and hence also the Ni^+/Al^+ ion intensity ratios are independent of x_{Ni} if two phases (L + γ, γ + γ', γ' + β, L + β, L + γ') are present in the alloy at the temperature of the measurement. This is not the case if the alloy consists of only one phase (e.g.: γ, γ', β). The dashed line (Fig. 5) representing the binary phase fields (L + γ), (L + γ'), and (L + β) results from extrapolation of the ion intensity ratios to the solidus temperatures obtained by differential thermal analysis. The three phase transitions shown in Fig. 7 by dots with error bars result from the experimental curves (Fig. 5) for x_{Ni} = 0.70, 0.74, and 0.75.

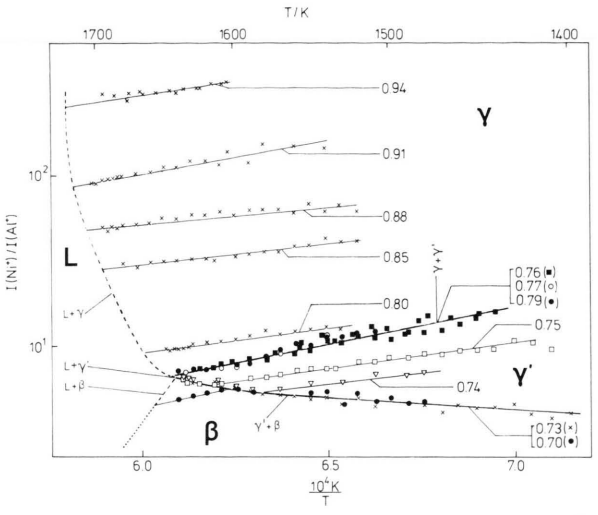

Fig. 5. Temperature dependence of the Ni^+/Al^+ ion intensity ratio, corrected for isotopic distribution, determined for different alloy compositions.

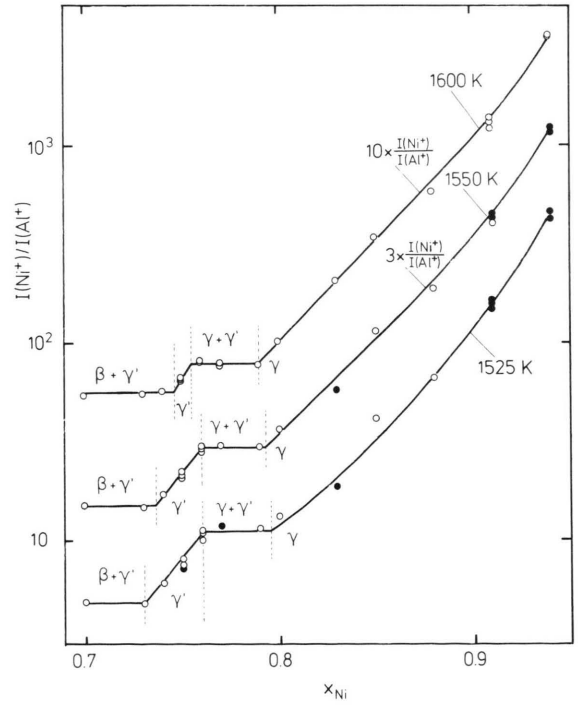

Fig. 6. Ni^+/Al^+ ion intensity ratios, corrected for isotopic distribution, at temperatures of 1525, 1550, and 1600 K determined for different alloy compositions (●, obtained by extrapolation).

The phase boundaries (β + γ')/γ', γ'/(γ + γ'), and (γ + γ')/γ between 1525 and 1600 K (Fig. 7) result according to the phase law as shown in Figure 6. Three isotherms are shown in this diagram as examples. Some of the points were obtained by extrapolation from $\log I(Ni^+)/I(Al^+)$ vs. $1/T$ plots. The dashed lines (Fig. 7) represent estimated uncertainties.

4. Discussion

Figure 7 shows the phase boundaries determined here by differential thermal analysis and Knudsen effusion mass spectrometry. In addition, the vaporization experiments indicate whether the alloys investigated consist of one or two phases (Section 3.2). On the basis of these results, complemented by selected literature data [3, 9], the phase diagram in Fig. 7 is obtained.

The given errors for the phase boundaries determined by Knudsen effusion mass spectrometry (Fig. 7) represent overall errors estimated from the evaluation procedure used (cf. Section 3.2). The overall error for the temperatures determined by differential thermal analysis is estimated to be smaller than $\pm$ 1 K, with the exception of the peritectic temperature obtained from a sample with x_{Ni} = 0.760. The overall error for this temperature value might be slightly higher than $\pm$ 1 K since it is not obtained by extrapolation to the base line (cf. Figure 4).

The DTA diagram obtained by cooling for an alloy with x_{Ni} = 0.760 (Fig. 4) is of particular interest. It clearly shows three exothermic reactions and indicates the liquidus, the peritectic and the eutectic temperatures. The values obtained for the eutectic and peritectic temperatures agree well with those resulting from the study of other samples (cf. Section 3.1). The two

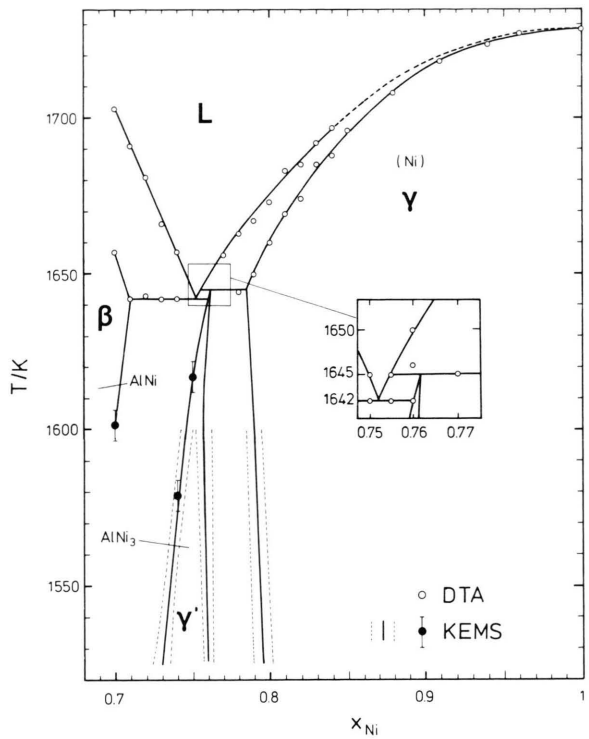

Fig. 7. Ni rich part of the Al–Ni phase diagram according to this work obtained by DTA and Knudsen effusion mass spectrometry, KEMS.

neighbouring samples referring to $x_{Ni} = 0.760$ with $x_{Ni} = 0.755$ and 0.770 show only two phase reactions like all the other samples investigated. This and the obvious high agreement between the data determined by Knudsen effusion mass spectrometry and differential thermal analysis (cf. Fig. 7) support the phase diagram of this work.

This phase diagram deviates from that given in the compilation by Hansen and Anderko [4] (Fig. 1), which was obtained by combining selected data from the works of Alexander and Vaughan [16], Taylor and Floyd [17], and Schramm [10]. In contrast to the phase diagram proposed by Hansen and Anderko, the diagram of this work shows the same phase equilibria and fundamental structure as that proposed by Schramm and disagrees with the results of Alexander and Vaughan as well as the diagram proposed by Taylor and Floyd. In this work the temperature for the beginning of the melting of the $(\gamma' + \gamma)$ phase field is higher than that of the $(\beta + \gamma')$ phase field as found by Schramm but not in [16] and [17].

The peritectic temperature, 1635 K, and the eutectic temperature, 1633 K, obtained by Schramm are lower by 10 and 9 K, respectively, than those obtained here. This difference is reduced by 4 K if one takes into account that Schramm took the melting temperature of nickel to be 1624 K while the value of the International Practical Temperature Scale [12] is 1628 K. The atom fractions, x_{Ni}, for the eutectic and peritectic points determined in this work (cf. Fig. 7) are by 0.009 smaller than those in Schramm's phase diagram [10]. This difference is supported by Schramm's observation of three exothermic reactions, corresponding to those shown in Fig. 4, for a sample with $x_{Ni} = 0.775$ (cf. Figure 7).

The $\beta/(\beta + \gamma')$, $(\beta + \gamma')/\gamma'$, $\gamma'/(\gamma' + \gamma)$, and $(\gamma' + \gamma)/\gamma$ phase boundaries have so far been determined by the analysis of quenched alloy samples at low temperatures (e.g. [10, 16, 17]). In contrast to that, these boundaries were determined here by measurements at the temperatures at which they exist. Changes in the alloy composition, which might happen during quenching, are thereby excluded.

The x_{Ni} values of the $(\gamma' + \gamma)/\gamma$ phase boundary obtained here for temperatures above 1525 K are by 0.004 smaller than those of Schramm [10]. They deviate from those of Alexander and Vaughan [16] by up to 0.03. The homogeneity range of $AlNi_3$ at 1550 K in this work, $0.735 < x_{Ni} < 0.760$, is shifted compared to [16], $0.724 < x_{Ni} < 0.750$, and [10] $0.742 < x_{Ni} < 0.771$. The phase boundaries of the $AlNi_3$ homogeneity range at our lowest temperature (1525 K) agree with those obtained by Taylor and Floyd [17] at their highest temperature (1423 K).

Acknowledgements

The authors thank the Alexander von Humboldt-Stiftung for granting a scholarship to enable M. M. to work at the KFA. V. V. thanks the International Bureau of KFA for financial support during his stay as a guest scientist under the bilateral agreement between India and the Federal Republic of Germany.

[1] B. H. Kear, Order-Disorder Transformations in Alloys, ed. H. Warlimont, Springer, Berlin 1974, p. 440.
[2] N. S. Stoloff, High-Temperature Ordered Intermetallic Alloys, ed. C. C. Koch, C. T. Liu, and N. S. Stoloff, Materials Research Soc., Pittsburgh (PA) 1985, p. 3.
[3] N. V. Ageev, Handbook of Binary Metallic Systems, Vol. 1, Israel Program for Scientific Translations, Jerusalem 1966, p. 214.
[4] M. Hansen and K. Anderko, Constitution of Binary Alloys, McGraw-Hill, New York 1958, p. 118.
[5] R. P. Elliott, Constitution of Binary Alloys, First Supplement, McGraw-Hill, New York 1965, p. 48.
[6] F. A. Shunk, Constitution of Binary Alloys, Second Supplement, McGraw-Hill, New York, 1969, p. 31.
[7] T. B. Massalski, Binary Alloy Phase Diagrams, Vol. 1, American Society for Metals, Ohio 1986, p. 140.
[8] P. D. Desai, J. Phys. Chem. Ref. Data **16,** 109 (1987).
[9] F. J. Bremer, M. Beyß, E. Karthaus, A. Hellwig, T. Schober, J.-M. Welter, and H. Wenzl, J. Crystal Growth, in press.
[10] J. Schramm, Z. Metallkunde **33,** 347 (1941).
[11] K. Hilpert et al., in preparation.
[12] Metrologia **5,** 35 (1969).
[13] K. Hilpert, in: Advances in Mass Spectrometry, Vol. 7 A, ed. N. R. Daly, Heyden & Son Ltd., London 1978, p. 584.
[14] K. Hilpert, Ber. Bunsenges. Phys. Chem. **83,** 161 (1979).
[15] See e.g.: K. Hilpert, Habilitationsschrift Technische Hochschule Darmstadt, Darmstadt 1981; Report from the KFA Jülich, Jül-1744, p. 11.
[16] W. O. Alexander and N. B. Vaughan, J. Inst. Metals **61,** 247 (1937).
[17] A. Taylor and R. W. Floyd, J. Inst. Metals **81,** 25 (1952).